JOURNAL OF GEOPHYSICAL RESEARCH, VOL. 102, NO. A5, PAGES 9741-9748, MAY 1, 1997

Large fluxes of auroral electrons in filaments of 100 m width

B. S. Lanchester,[1] M.H. Rees,[1] D. Lummerzheim,[2] A. Otto,[2] H.U. Frey,[3,4] and K.U. Kaila[5]

Abstract. The combination of high time and space resolution measurements in the magnetic zenith (optical and radar) and detailed modeling of the ionospheric response to auroral particle precipitation has produced the new result that most of the energy density in a bright arc resides in an extremely narrow filament, embedded in a broader feature. We are able to show that the narrow filaments, of the order of 100 m width, are produced by monoenergetic beams of electrons, whereas the surrounding emissions of lower energy density are produced by broad spectral distributions. The new result is achieved by combining different energy spectra as input to an auroral model and comparing the resulting electron density profiles with those measured with the European incoherent scatter radar at 0.2 s time resolution. The result is dependent on the optical evidence that the narrow energetic beams do not fill the fields of view of the detectors, i.e. both photometer and radar. Agreement between the observed structure, scale lengths, and evolution of the aurora and modeled predictions suggests that transient parallel electric fields are important acceleration mechanisms above the ionosphere.

Introduction

The energy density in auroral structures can be derived from (1) the brightness of the optical aurora (including ultraviolet emissions), (2) the flux of energetic electrons and ions that produce the aurora, and (3) the enhancement in electron density resulting from increased auroral ionization rate. All three methods are valid, each with important caveats. Optical instruments measure surface brightness, using the assumptions that the field of view of the device is completely and uniformly filled and that the aurora does not change or move during the measuring interval. These assumptions are also made for radar measurements that provide the electron density of method 3. Energetic particle fluxes are measured by detectors on board rockets or satellites, and there is not much choice but to assume that the energy and pitch angle characteristics of the flux do not change during the sampling time. At an orbital speed of several kilometers per second this assumption requires extremely high time resolution detectors to avoid ambiguities in the measurements.

Viewed in the magnetic zenith, auroral arcs are usually filamented and rarely still. As a result, none of the three observational methods listed above is able to measure the characteristics of individual auroral arc elements that can be identified on high-resolution video images. Instead, radar and photometric measurements yield average characteristics over the respective fields of view, while satellite and rocket measurements give averages along the spacecraft track. In addition to the underestimation of the energy density there is the possibility that if more than one arc element is in the field of view of a detector, then the input energy spectrum will be made up of more than one distribution.

McFadden et al. [1990] used a large set of measurements from two sounding rockets fired into a narrow (10 km) discrete arc, which demonstrated the complexities of such structures. They concluded that there was a need for much higher resolution measurements using multiple spacecraft. Since then, several instruments on the Freja satellite with very high time resolution have enabled a large data set to be used to look for small-scale variations in electron precipitation and auroral plasma. *Boehm et al.* [1994, 1995] have described inverted-V structures of 1-5 km scale sizes and a boundary of only 10 m in electron flux, with interesting implications for the corresponding optical signatures, which in this case would have been weak at around 1 kR. Other subkilometer structure in low-energy thermal plasma also measured by Freja instruments has been reported by *Knudsen et al.* [1994]. Since fine structure is so often observed in auroral forms, the physical processes that produce it must be incorporated in the theory of auroral arc production [*Borovsky,* 1993]. One of the parameters used as a starting point for theoretical analysis is the energy flux associated with an arc element. We report here our analysis of radar and optical measurements of an intense auroral event that illustrates the limitations of the instruments. Detailed modeling, however, leads to a reasonable explanation of the observations that has not been proposed quantitatively before.

Observations

Radar, photometric, and imaging data were acquired at the European incoherent scatter site near Tromsø, Norway, during an auroral campaign in January 1995. The radar experiment

[1]Department of Physics, University of Southhampton, Southhampton, England.
[2]Geophysical Institute, University of Alaska, Fairbanks.
[3]Max-Planck-Institut für Extraterrestische Physik, Garching, Germany.
[4]Now at Space Sciences Laboratory, University of California, Berkeley.
[5]Department of Physics, University of Oulu, Oulu, Finland.

Paper number 97JA00231.
0148-0227/97/97JA-00231$09.00

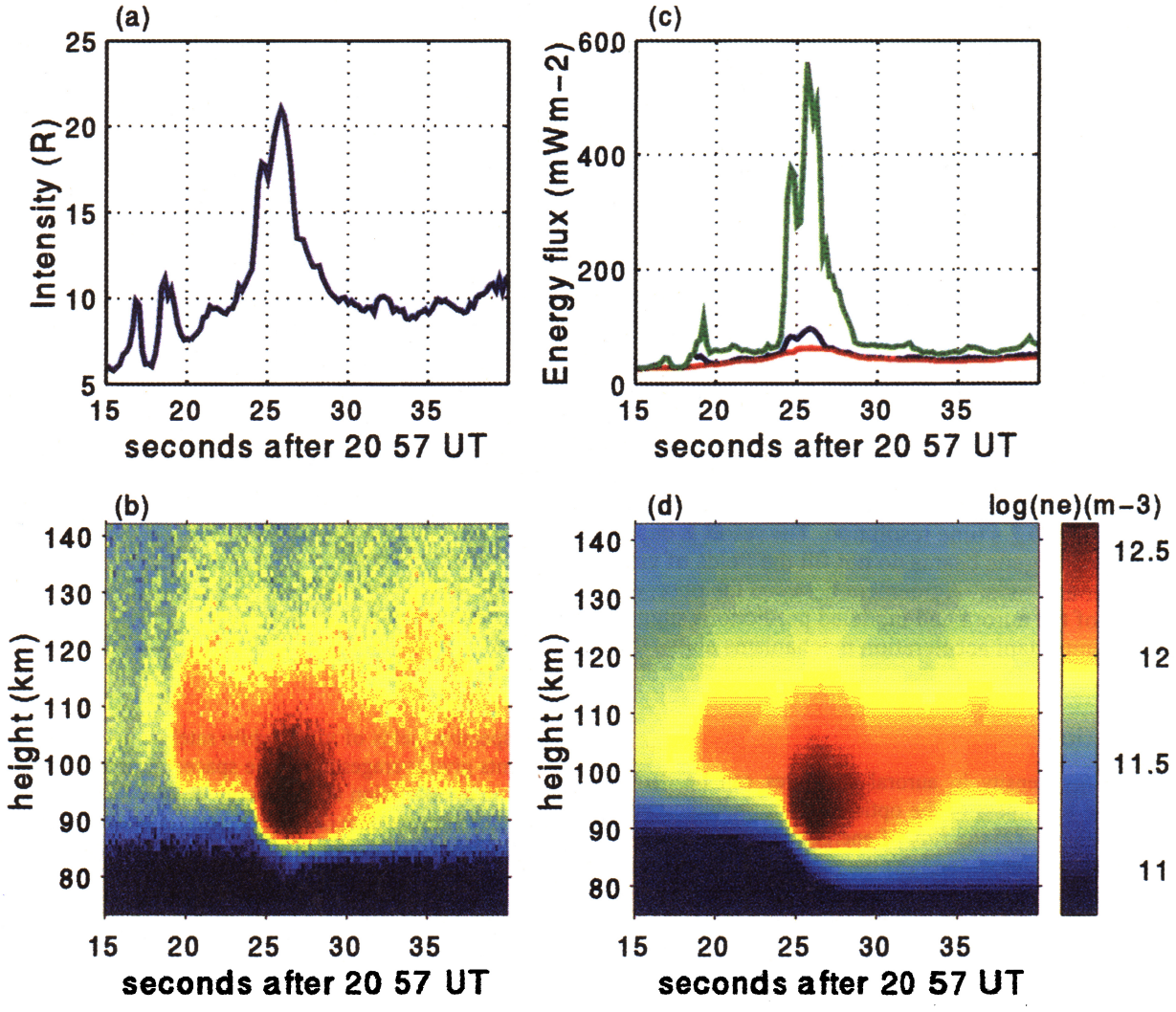

Plate 1. (a) Measured 427.8 nm emission (0.2 s resolution), corrected for scattering and extinction. (b) Measured electron density (0.2 s resolution) from the EISCAT radar, January 30, 1995. (c) Energy flux required as input (green line) to obtain a good fit between the measured and modeled electron density. The red line is the contribution to the flux from a broad energy distribution, which accounts for the background emission. The difference between the two is the energy flux residing in the very narrow and bright filament. The blue line is the (inadequate) flux estimated from the photometer measurement of (a). (d) Modelled electron density using the input of (c).

(PULSE) was designed to measure rapidly varying auroral events. In the present analysis, only the power profile measurement, between 75 and 145 km with 1.05 km range resolution, is used. These data were obtained at 0.2 s resolution by using a Barker coded modulation. The filter photometer had a 0.5° field of view, which was coincident with the field-aligned radar beam. Two image-intensified CCD cameras were operated at 25 frames/s with fields of view of 86° times 64° and 15° times 21°. Both cameras used a short-wavelength cutoff filter at 650 nm, eliminating the long-lived emissions from atomic oxygen, to allow the prompt emission of N_2^+(Meinel) and N_2 1 PG bands to produce a very sharp image [*Frey et al.*, 1996].

The real time images were searched for examples of distinct filamentary structure, which passed through the magnetic zenith. Many examples were identified, and we report here the analysis of a 25 s interval that ocurred on January 30, 1995 at 2057 UT. The photometer isolated the 427.8 nm band emission of the N_2^+ 1 NG (0,1) system. The measured photon emission rates, corrected for scattering and extinction in the lower atmosphere, are shown in Plate 1a. Electron density profiles were derived from the backscattered power of the EISCAT radar. The density during the 25 s interval increased to 5×10^{12} m^{-3} at 92 km, as shown in Plate 1b. Exact time coincidence of the maxima in the 427.8 nm emission rate and the electron density is not expected, because the optical emission at this wavelength is a prompt emission resulting from direct impact ionization and excitation, whereas the electron density is described by the time dependent continuity equation, involving production and loss terms. Horizontal plasma drift is not expected to be significant at these heights below 100 km, where the ions are controlled by the neutral wind rather than by the convection electric field. The delay between the prompt emissions and the rise in electron density has not been noted previously, because radar data are generally acquired at resolution of 1s or longer, whereas our

data are at 0.2 s resolution, as are the photometer measurements. The exact alignment and comparable surface area of the radar and photometer fields of view are also essential for this effect to be seen. Additional evidence for this time delay is provided by the sequence of images from the narrow-angle camera, with pixel resolution of 50 m. The response of the photometer as an arc element enters the region is simultaneous with the optical image, but the electron density does not rise to its peak until the filament has left the field of view. This effect is seen best when the arc element passes straight through the beam, as happens at 2057:18 UT, with the maximum in electron density occurring more than a second later when the element has left the beam. The next increase in emission rate which occurs at 2057:24 UT, results from the same arc returning into the beam (from a few kilometers north of it), brightening while in the beam, then moving on again to the north. This brightening in the beam corresponds to the maximum measured electron density, with deepest penetration to 92 km and therefore more energetic electron precipitation. During the whole interval the very bright elemental arc was embedded in an extended region of auroral luminosity.

Analysis

The auroral model used as a basis for this work has been described by *Lanchester et al.* [1994]. Refinements to the model have been made to analyze the improved measurements from this campaign. The photometer field of view, reduced from 2° to 0.5°, is now equivalent to the EISCAT beam width. This means that the 427.8 nm emission rate can be used, in principle, as input to the model as a measure of the incident energy flux. We adopted a conversion factor of 220 R/mW m^{-2}, which we derived from a set of electron transport calculations [*Lummerzheim and Lilensten,* 1994]. The conversion factor depends on the characteristic energy of the precipitating electron flux, or equivalently, the height of maximum energy deposition and the ratio of N_2 density to total density. The factor can vary between 220 and 280 R/mW m^{-2}; the small value is appropriate for the characteristic energy of this event.

In addition to a time history of electron energy flux, the analysis requires a peak energy and spectral shape, usually given as a Maxwellian or Gaussian distribution of specified half width. The latter can be used to represent a "monoenergetic" electron beam. The peak energy can be estimated from the height of the maximum in electron density but shifted back in time to match the delay mentioned above. At each time step (here 0.2 s) the electron transport equation is solved, giving degraded electron spectra from 500 km to 75 km height and profiles of auroral ionization, excitation, and electron heating rates. These are the input to the ion chemistry part of the model, in which the time dependent coupled continuity equations for all important positive ions and minor neutral species are solved. The electron density is the sum of the positive ion densities. The electron temperature is obtained by solving the local electron energy equation. For different input energy distributions the resulting electron density profiles can be compared with those measured with the radar and so can establish the most likely energy spectra in the arc when it is in the detectors' fields of view.

To model the electron density of Plate 1b, initially we took as input the energy flux derived from the 427.8 nm measurements of Plate 1a, with a Maxwellian spectral shape for most of the 25 s interval. Only the 3 s interval between 24 and 27 s was given a narrow Gaussian distribution with 10% half width. The justification for adopting this spectral shape was the sharp gradient in the electron density below the maximum at these times of increased signal. The result of this first model run produced peak electron densities of 2×10^{12} m^{-3} (12.3 on log scale), well below those measured, but the most obvious deficiency was the lack of electron density above the height of the peak. The Gaussian-shaped energy spectrum at the time of the intense event was not adequate as sole input. The input spectrum requires, in addition, a significant contribution from lower-energy electrons. Therefore the same input energy flux was divided into two contributions, with the Maxwellian background throughout the interval, and a Gaussian flux was added at the times of increased luminosity when the central core of the arc was in the fields of view of the detectors.

The resulting density profiles from the combined spectra were closer in shape to the measured electron density profiles, but the peak values were still only 2×10^{12} m^{-3}. Therefore the total energy flux inferred from the 427.8 nm emission rate measured by the photometer was not adequate. It appeared from inspection of the individual profiles that the energy flux for the Maxwellian background was reasonable, but the monoenergetic flux was not. The implication is that the monoenergetic contribution to the 427.8 nm emission was not spatially resolved by the photometer. On further inspection of the images from the narrow-angle camera it is clear that the core of the arc was at times extremely bright, at most a few pixels in width. It is therefore reasonable to assume that the narrow filament did not fill the field of view of the photometer and to multiply the monoenergetic component of the energy flux by a compensating factor, which could be estimated from the model results.

The "best fit" input energy flux is shown by the green line in Plate 1c. The contribution from the Maxwellian background is given by the red line. The total flux derived from the photometer measurements is shown by the blue line and is very nearly the same as the background flux. The resulting electron density is shown in Plate 1d. Here the peak electron densities of 5×10^{12} m^{-3} are reproduced, as is the time delay between the arrival of the light in the beam and the subsequent rise in electron density. More importantly, however, the shape of the profiles is well matched throughout. Figure 1a shows the excellent match between measured and modeled electron density at the time of the maximum at 2057:26.8 UT. By making the assumption that the narrow filament in the central core of the arc contains most of the energy flux in the arc, here in excess of 500 mW m^{-2}, the measured and modeled electron densities are almost identical. By simple geometry it is clear that if the energy density is multiplied by a factor of 10 then the area of the detector field of view filled by the monoenergetic beam must be one tenth of the total. This calculation puts a width of the order of 100 m to the energetic electron beam.

The estimate of the width of the monoenergetic electron beam is supported by the optical evidence of the narrow angle camera, shown in Figure 2. The circle gives the position of the photometer and radar fields of view. Its diameter at the

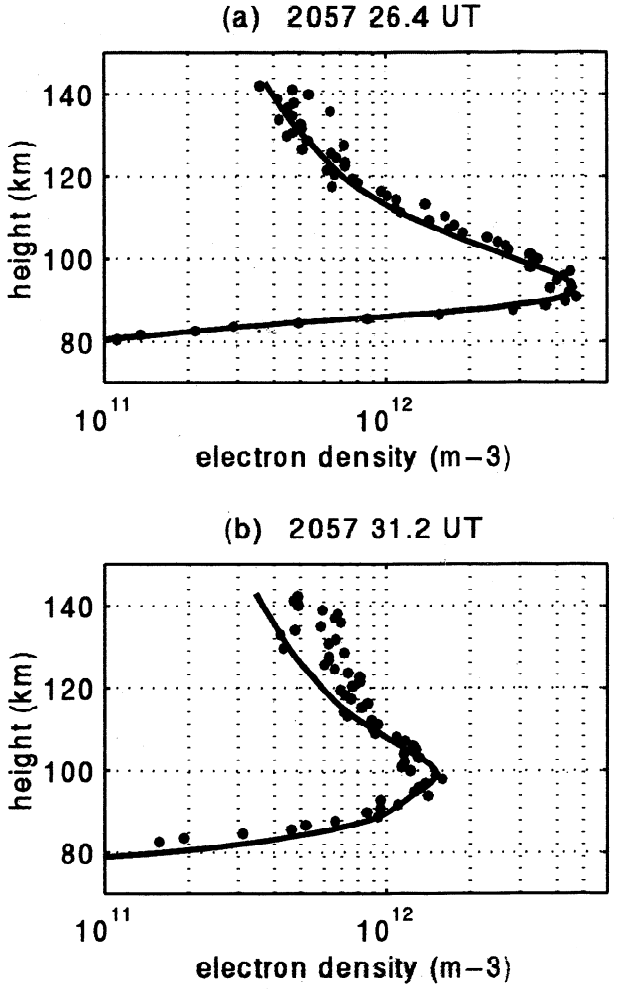

Figure 1. (a) Measured (circles) and modeled electron density profiles at the time of maximum density, with total energy flux in excess of 500 mW m^{-2}, mostly supplied by the monoenergetic electrons. (b) Measured (circles) and modeled electron density profiles when the narrow bright filament was not in the beam (see Figure 2). Most of the energy flux at this time is supplied by the Maxwellian distribution of the wider arc.

height of the peak emission is about 900 m, and the pixel resolution is 50 m. It is important to understand the problems of contrast and dynamic range in interpreting these images. The number in the left-hand corner (say a) relates to the exposure time t, where t = 40 ms x 2^a (a = -13.....+13). The camera gain is held at a constant value for the run time, but the exposure time is changed to accommodate the variations in light intensity with time. The exposure time in this frame is as short as 2.5 ms. In this case the arc moved into the zenith and brightened so suddenly that the first part of the event had too long an exposure time and completely saturated across the width of the broader arc. The frame shown here is a few seconds later (2057:31 UT), when the core of the arc had moved out of the zenith and the exposure time adjusted to the maximum brightness of the image. However, there is still a large light signal from this neighboring region, as indicated by the gray background. Within this extended region of luminosity, other fine structure could be present but not be visible on the images because of the limited dynamic range.

The profiles of Figure 1b show that the peak electron density at 2057:31 UT, corresponding to the frame shown in Figure 2, is still very large in the region near the bright narrow filament, in excess of 1 x 10^{12} m^{-3}. At this time the input energy flux is mostly of a Maxwellian distribution, with some input from a narrower distribution. Further adjustments could be made to the low energy contribution for an even better fit. As can be seen from the color plot of Plate 1b, during the latter part of the analyzed interval the electron density has a secondary broad maximum between about 120 and 135 km. This could result from plasma drifting into the field of view from adjacent bright regions of aurora [*Palmer*, 1995], rather than another energy distribution in the precipitating particles.

The values of peak energy used in the model for both Maxwellian and Gaussian contributions determine the height of peak ionization rate and are necessary for fitting the height profiles. However, this parameter is not as important as the energy flux and its division into two spectral contributions in producing the result of interest here. For information, in Figure 1a the peak energy of the monoenergetic beam is 22 keV, and that of the Maxwellian contribution is 8 keV.

Discussion

This work, combining modeling with measurements from several instruments, provides the first real evidence that the energy in a very bright auroral arc is mostly in a very narrow (<100 m) beam of monoenergetic electrons, embedded in a broader region of electron precipitation with a spread of energy. This result is important input for theoretical work on the production of auroral arcs above the ionosphere and the mechanisms that produce field-aligned currents with such fine structure within the larger-scale feature. What now needs to be addressed is the inference that two separate scale sizes are operating together. It appears that the energy of the larger-scale structure is consistent with a process that scatters electrons into the loss cone. The acceleration mechanism for the larger-scale feature could produce the inverted-V distributions reported by *Lin and Hoffmann* [1979] and is consistent with most of the generator processes examined by *Borovsky*

Figure 2. Image from the narrow-angle TV at 2057:31.5 UT. The position of the photometer and radar fields of view is marked. The field of view is 38 km times 28 km, with north to the right and east at the top.

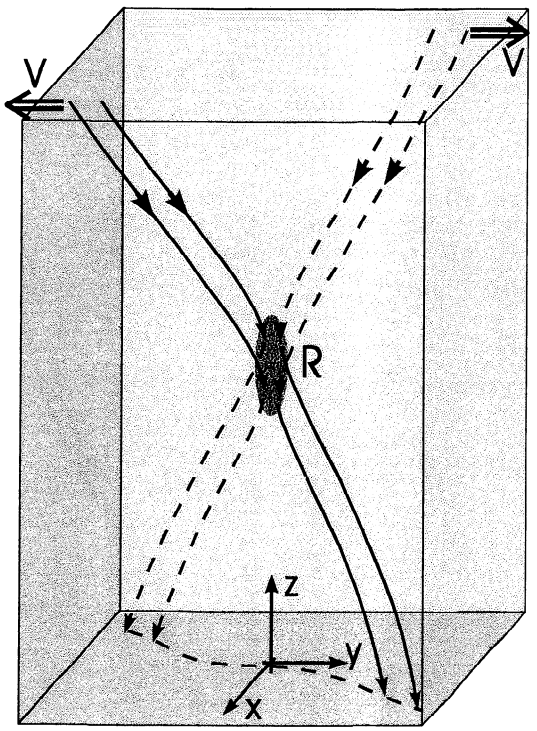

Figure 3. Sketch of the magnetic field geometry resulting from a localized acceleration region in a field-aligned current layer. Plasma flow in the magnetosphere (associated with the top of the box) generates the magnetic shear and a field-aligned current layer, and magnetic reconnection in the acceleration region (R) connects magnetic flux from the back to the front. The field-aligned electric field maps along the deformed magnetic field to the bottom (associated with the ionosphere) into a thin elongated region.

[1993]. *Otto and Birk* [1993] have suggested that if the acceleration process is viewed as a decoupling between the magnetosphere and ionosphere, then it follows that the decoupling process is a multiscale process. According to *Borovsky* [1993], no model at that time predicted the observed very narrow features. Since Borovsky's review of the subject a new theoretical model has been developed by *Otto and Birk* [1994] that is capable of producing thin arcs. A description of this model follows.

Field-aligned currents are a fundamental property of the magnetosphere-ionosphere interaction. Satellite measurements have shown that thin current sheets are embedded within the large-scale region 1 and region 2 currents. In the sketch in Figure 3 such a current sheet lies in the y-z plane at x = 0. The dipole magnetic field is in the z direction, and the current implies a shear in the magnetic field, which is oppositely directed on either side of the current sheet. The magnetic perturbation and the current layer are generated by magnetospheric convection indicated at the upper boundary of the box in Figure 3. Both the magnetic shear and the current increase if the foot point motion of magnetic field lines in the ionosphere (bottom boundary in Figure 3) cannot follow the convection in the magnetosphere. If the current density exceeds some threshold value, turbulent flow may result, leading to the generation of electrostatic or electromagnetic waves, which produce a collisionless resistivity (indicated by R in Figure 3), and resulting in a parallel electric field. The presence of a localized parallel electric field in the current layer implies a topological readjustment of the magnetic field configuration, often named reconnection. This process maps the foot point loci of magnetic field lines into the direction of the applied convection, thereby providing a very efficient relaxation of the configuration. In the sheared field configuration, the parallel electric field maps to a thin elongated filament and provides the acceleration for the monoenergetic flux of electrons. The process is highly time dependent.

We present here some of the central results of this model, using a three-dimensional multifluid simulation (electron, ion, and a neutral fluid component [*Birk and Otto,* 1996]). A publication of detailed results is in preparation. In the simulation the lower boundary in z is located at the altitude of the lower *F* region, and the ionosphere contains a gravitationally bound neutral component, allowing for a realistic model of plasma-neutral friction and collisional resistivity. Ohm's law includes a Hall term, although this appears to be of minor importance for the dynamics in the acceleration region. The simulation is carried out in a three-dimensional box similar to the one illustrated in Figure 3 with a size of 30 by 30 km in x and y at the ionospheric boundary (the convergence of the dipole field implies a size of about 100 by 100 km at the magnetospheric boundary). The vertical size is approximately 2 R_E. Boundary conditions are such that plasma can enter and exit the box at x = -15, x = 15 respectively, and at z = 12,000. The lower boundary of z represents a solid wall, and line symmetry is chosen at y = 0, x = 0, and at y = 30, x = 0 (all units are in kilometers). The simulation starts with a preexisting current layer centered at x = 0 with a thickness of 2 km at ionospheric altitudes (which is not necessary but saves computer time). A shearing plasma flow (of amplitude 20 km/s) is applied at the magnetospheric boundary as illustrated in Figure 3.

In the simulation a field-aligned electric field is generated by a resistive term in Ohm's law if the current density surpasses a threshold value of about 30 $\mu A\ m^{-2}$. A small-amplitude perturbation is applied at time t = 0 to initialize the formation of the acceleration region. The maximum value of the field-aligned electric field during the simulation is about 1 $mV\ m^{-1}$. The vertical extent is about 3000 km at an altitude of roughly 1 R_E, and the horizontal size is approximately 10 km. It is clear that the results depend quantitatively on these values. However, the morphology and qualitative evolution require only that the acceleration region be localized in space. For this process, *Otto and Birk* [1993] have shown that the convection electric field scales with the horizontal magnetic field perturbation $B_\perp$, the field-aligned electric field scales with $B_\perp^2$, and the timescale is proportional to $1/B_\perp$. For the presented results the horizontal magnetic field perturbation is about 40 nT. Freja observations have shown very localized perturbations of up to 200 nT such that the field-aligned potential difference could be a factor of 25 larger and the timescale a factor of 5 faster than that shown in the following results.

As a central result of the simulation the sequence of plots in Figure 4 shows the time evolution of a discrete arc based on the above model using a three-dimensional, time dependent, numerical simulation. Only a part of the entire simulated space is shown in the figures. Each plot presents the field-aligned electric potential difference mapped to the ionospheric boundary in the simulation. The mapping is obtained by an integration of the parallel electric field along

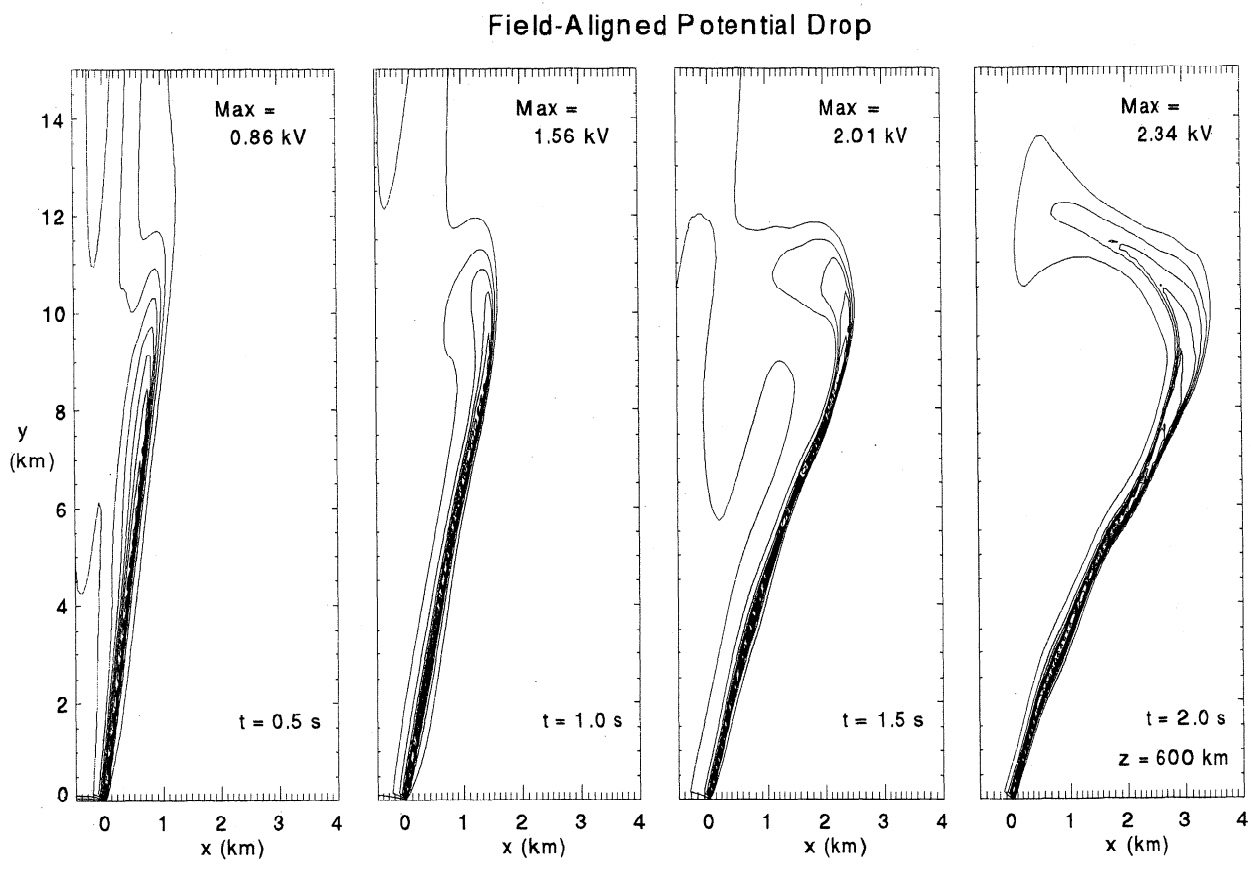

Figure 4. Time evolution of the field-aligned electric potential drop obtained with a three-dimensional simulation of magnetic reconnection resulting in a localized auroral acceleration region. Each plot shows 11 contour lines spaced uniformly between zero and the maximum value for electric potential drop shown on each plot. The plots show a horizontal cut through the ionosphere at an altitude of about 600 km and are separated by 0.5 s in time. The potential structures are symmetric with respect to the origin at x=0, y=0.

magnetic field lines starting from the ionospheric boundary. One length unit in the x or y direction corresponds to approximately 1 km distance. The time separation between two consecutive images is about 0.5 s such that the entire sequence is about 2 s . The maximum potential difference for this case is approximately 2.3 kV. The value of the maximum potential depends on the horizontal magnetic field perturbation and thus on the driving force in the magnetosphere. For the chosen setup the potential starts to saturate toward the end of the sequence shown in Figure 4. Along the thin layer the variation of the maximum potential is rather small.

The contour plots show the formation, evolution, and rapid motion of a very thin (approximately 100 m) potential structure. The thinning is caused by a localized acceleration source that is embedded in a field-aligned electric current region. At an altitude of about 6000 km the acceleration region has a width of a few kilometers in the simulation. The thin potential structure is embedded in a much wider (1 km to several kilometers) field-aligned current region. Because of the presence of the parallel electric field the potential structure is not frozen into the plasma. It can be seen from the sequence of plots that parts of the potential structure move with a speed of about 2 km/s. In the model the motion normal to the filament (x in Figure 3) is faster for larger parallel electric fields and higher energies of the monoenergetic particle flux. (It also depends on the altitude of the parallel field.)

Further simulation results relevant to the observation of thin arcs are presented in Figure 5. The first two plots show the distribution of field-aligned current above the *F* region at times t = 1 s and t = 2 s. The original current (and the current generated by the sheared plasma velocity at the magnetospheric boundary) is centered at x = 0. Solid contours show the large values of the absolute current densities, and dashed contours show values smaller than 40% of the maximum. The plots show a thinner current structure (1 km) embedded in a wider (4 to 6 km) current region. The thinner current filament is found approximately at the location of the potential structure and follows the potential structure during the simulation. Although this current filament is rather thin, it is much thicker than the 100 m potential structure consistent with observations, indicating that only a fraction of the electrical current is actually carried by energetic electrons [*Lanchester and Rees,* 1987]. If we assume that electron precipitation occurs in the region of field-aligned current, then the presence of the very thin potential structure in the extended region of field-aligned current is consistent with the present observation showing a thin region of high-energy precipitation embedded in a much larger region of lower-energy precipitation.

The third plot in Figure 5 shows horizontal plasma convection in the same region as the field-aligned current plots for time t = 2 s. Comparing the convection with the corresponding potential structure in Figure 4 demonstrates fast

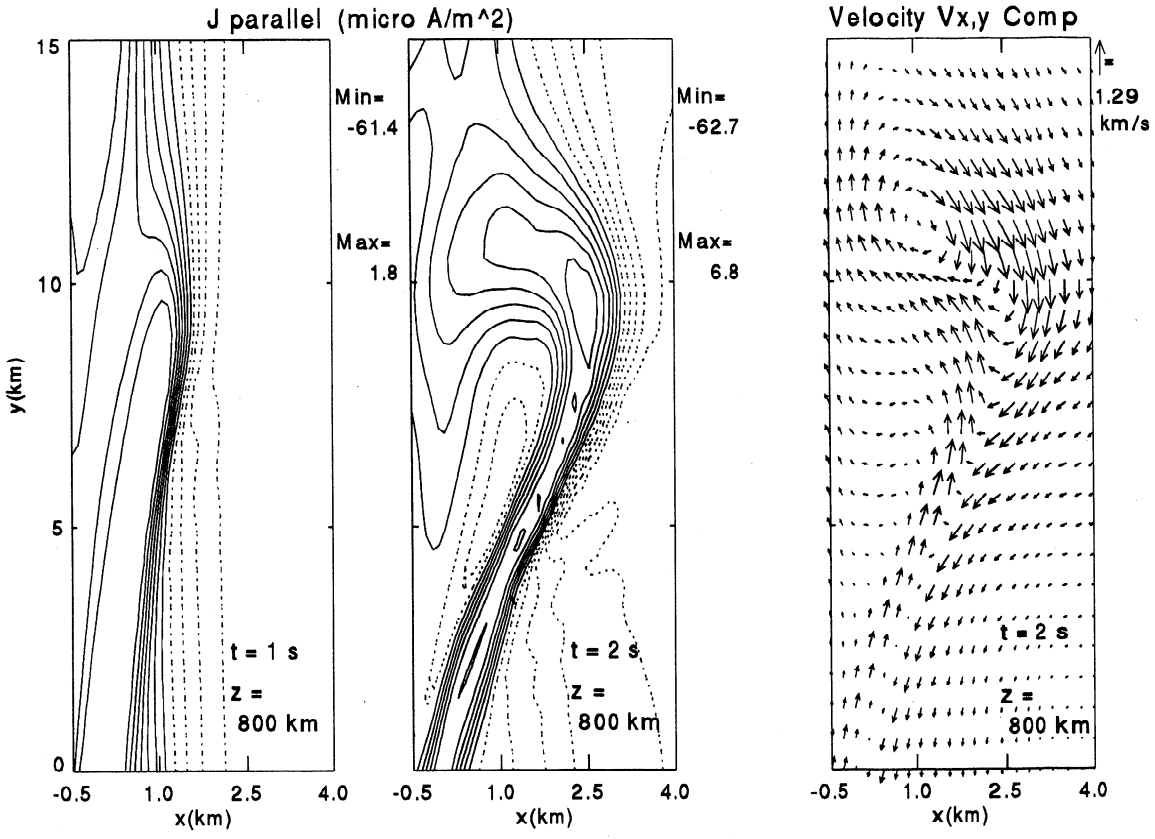

Figure 5. Contours of field-aligned current density for time (left) t = 1 s and (center) t = 2 s and (right) arrows indicating the plasma velocity in a horizontal plane directly above the ionosphere as a result of the simulation. Contour lines are spaced by approximately 6 μA m^{-2}, and the transition from solid to dotted is chosen at 40% of the maximum absolute current density. Solid contours indicate larger absolute current density. The maximum convection velocity in the third panel corresponds to about 1.3 km/s.

tangential flow in the immediate vicinity of the potential structure. The magnitude of this flow is approximately 1 km/s. Compared with the tangential flow, the component perpendicular to the thin structure is small (a few hundred meters per second). It is obvious that this flow is insufficient to explain the fast motion of the structure in the perpendicular direction, implying a violation of the frozen-in condition and the presence of a field-aligned electric field.

In the event discussed here the auroral arc element moves through the field of view of the instruments with rapid variations in its velocity, sometimes as fast as 8 km/s normal to its length. Images from the CCD camera (25 frames/s) show that the displacement is not uniform in space and time and that a fold develops for a few seconds near the middle of the arc element in the field of view. This behavior is consistent with a localized acceleration process, as assumed in the model. The large measured velocities of the arc filament are much greater than those usually associated with the background plasma convection velocity and suggest that the corresponding particle precipitation is not frozen into the magnetic field [*Haerendel et al.*, 1993]. *Lanchester et al.* [1996] have previously measured velocities of this magnitude of optical features along the length of an arc element and, more importantly, have also reported large but short-lived plasma velocities of several kilometers per second beside the bright features in the arc. The corresponding large electric fields (400 mV/m) were considered to be related to the temporal brightenings in the arc and therefore superimposed on the background electric field. In this earlier set of observations from the same site at Tromsø a fortunate conjunction of events allowed the EISCAT radar to measure the plasma velocity tangential to the arc at 3 s resolution. The radar sampled the plasma beside and very close to the bright arc for 30 s. In the present observations the plasma velocities are not useable at this resolution, as the conditions in the radar field of view varied too much during the interval of interest.

Although the peak energies of the monoenergetic electron beam in the present case were large (22 keV) and the narrow arc element penetrated to 92 km, we have many other examples of much weaker narrow structures that do not fill the fields of view of the radar and photometer and that may relate to the observations of *Boehm et al.* [1995]. Therefore we believe that the presence of monoenergetic beams of electrons is not confined to very bright elemental arcs, though these are the more spectacular and display more rapid movements and wave motions along their length. The fact that even so-called "diffuse" aurora is structured when viewed in the magnetic zenith has implications in interpreting measurements that assume a uniformly filled detector. There are also theoretical implications regarding acceleration processes, which we have begun to address here.

The simulation results are consistent with the observed thickness and the fact that the thin arc is embedded in a much broader precipitation and field-aligned current region. They

are also consistent with the expectation of fast tangential flow along discrete arc structures [*Lanchester et al.*, 1996]. These morphological properties are not expected to depend on boundary conditions or the magnitude of the field-aligned electric field. Quantitatively, the model underestimates the energy of the monoenergetic component by about a factor of 10 and the maximum perpendicular speed of the thin arc by a factor of 3 to 4. As mentioned above, the velocity of the potential structure is proportional to the horizontal magnetic field perturbation, and the field-aligned electric field is proportional to the square of this magnetic field. Parameters of the simulation lead to a horizontal field of 30 to 40 nT in the acceleration region. These numbers indicate a true horizontal magnetic field component of about 3 times the simulation value in the acceleration region (or a much lower plasma density than the 10 cm^{-3} assumed in the simulation). Such a larger field perturbation can be caused by a faster driving velocity at the magnetospheric boundary and/or by a larger threshold for the formation of the field-aligned electric field.

This new work advances the theory of auroral arc production, in particular the production of rapidly varying and very narrow (100 m) auroral elements in which reside very large energy fluxes (>500 mW m^{-2}), but there is more work to be done on less spectacular auroral events, when fine-scale structure is observed.

Acknowledgments. We thank the director and staff of the EISCAT Scientific Association, along with the U.K. campaign team, for help in running the EISCAT experiment. We thank Tauno Turunen for the design of the EISCAT experiment and E. Rieger, H. Loidl, and H. Holma for their contribution to the optical measurements. Jonathan Palmer was responsible for the development of the auroral model in his doctorate work at Southampton. Thanks are due to him and to Paul Field for help during the present work. B.S.L. is supported by a grant from the PPARC in the United Kingdom. Work by M.H.R., D.L., and A.O. is supported by the NSF grant ATM94-09485, and A.O. acknowledges support by the NASA Space Physics Theory grant NAG 5-1504 and a PPARC Visiting Fellowship at the University of Southampton. The EISCAT Scientific Association is supported by the Suomen Akatemia of Finland, Centre National de la Recherche Scientifique of France, Max-Planck Gesellchaft of the Federal Republic of Germany, Norges Almenvitenskapelige Forskningsråd of Norway, Naturvetenskapliga Forskningsrådet of Sweden, and the Particle Physics and Astronomy Research Council of the United Kingdom.

The Editor thanks A. W. Yau for his assistance in evaluating this paper.

References

Birk, G. T., and A.Otto, A three-dimensional plasma-neutral gas fluid model, *J. Comput. Phys.*, *125*, 513-525, 1996.

Boehm, M. H., G. Paschmann, J. Clemmons, G. Haerendel, L. Eliasson, and R. Lundin, Freja observations of narrow inverted-V electron precipitation by the two-dimensional electron spectrometer, *Geophys. Res. Lett.*, *21*, 1895-1898, 1994.

Boehm, M. H., J. Clemmons, and G. Paschmann, Freja observations of a ten-meter boundary within monoenergetic auroral electron precipitation, *Geophys. Res. Lett.*, *22*, 69-72, 1995.

Borovsky, J. E., Auroral arc thicknesses as predicted by various theories, *J. Geophys. Res.*, *98*, 6101-6138, 1993.

Frey, H.U., W. Lieb, O.H. Bauer, H. Höfner, and G. Haerendel, CCD-camera system for stereoscopic optical observations of the aurora, *Proc. SPIE Int. Soc. Opt. Eng.*, *2863*, 460-466, 1996.

Haerendel, G., S. Buchert, C. la Hoz, B. Raaf, and E. Rieger, On the proper motion of auroral arcs, *J. Geophys. Res.*, *98*, 6087-6099, 1993.

Knudsen, D. J., B. A. Whalen, A. W. Yau, M. J. Greffen, A. I. Eriksson, N. Lloyd, M. Boehm, J. Clemmons, and L. J. Blomberg, Sub-kilometre thermal plasma structure near 1750 km altitude in the polar cusp/cleft, *Geophys. Res. Lett.*, *21*, 1907-1910, 1994.

Lanchester, B. S., and M. H. Rees, Field-aligned current reversals and fine structure in a dayside auroral arc, *Planet. Space Sci.*, *35*, 759-768, 1987.

Lanchester, B. S., J. R. Palmer, M. H. Rees, D. Lummerzheim, K. U. Kaila, and T. Turunen, Energy flux and characteristic energy of an elemental auroral structure, *Geophys. Res. Lett.*, *21*, 2789-2792, 1994.

Lanchester, B. S., K. Kaila, and I. W. McCrea, Relationship between large horizontal electric fields and auroral arc elements, *J. Geophys. Res.*, *101*, 5075-5084, 1996.

Lin, C. S., and R. A. Hoffman, Characteristics of inverted-V events, *J. Geophys. Res.*, *84*, 1514, 1979.

Lummerzheim, D., and J. Lilensten, Electron transport and energy degradation in the ionosphere: evaluation of the numerical solution, comparison with laboratory experiments and auroral observations, *Ann. Geophys.*, *12*, 1039-1051, 1994.

McFadden, J. P., C. W. Carlson, and M. H. Boehm, Structure of an energetic narrow discrete arc, *J. Geophys. Res.*, *95*, 6533-6547, 1990.

Otto, A., and G.T. Birk, Formation of thin auroral arcs by current striation, *Geophys. Res. Lett.*, *20*, 2833-2836, 1993.

Otto, A., and G. T. Birk, Formation of thin discrete auroral arcs, in *Substorms 2: Proceedings of the Second International Conference on Substorms*, edited by J.R.Kan, J.D.Craven, and S.-I.Akasofu, p.127, Univ. of Alaska, Fairbanks, 1994.

Palmer, J.R., Plasma density variations in the aurora, Ph.D. thesis, Univ. of Southampton, Southampton, England, 1995.

H. U. Frey, Space Sciences Laboratory, University of California, Berkeley, CA 94720-7450, U.S.A. (e-mail: hfrey@ssl.berkeley.edu)

K. U. Kaila, Department of Physics, University of Oulu, SF-90570 Oulu, Finland. (e-mail: kari.kaila@oulu.fi)

B. S. Lanchester and M. H. Rees, Department of Physics, University of Southampton, Southampton, SO17 1BJ, UK. (e-mail: bsl@phys.soton.ac.uk; mhr@phys.soton.ac.uk)

D. Lummerzheim and A. Otto, Geophysical Institute, University of Alaska, Fairbanks AK 99775. (e-mail: ao@tanana.gi.alaska.edu; lumm@odin.gi.alaska.edu)

(Received October 9, 1996; revised January 21, 1997; accepted January 22, 1997.)